



Article

Amino-Functionalized Fe₃O₄@SiO₂ Core-Shell Magnetic Nanoparticles for Dye Adsorption

Chun-Rong Lin ^{1,*}, Oxana S. Ivanova ^{2,3,*} , Dmitry A. Petrov ², Alexey E. Sokolov ^{2,3} , Ying-Zhen Chen ¹, Marina A. Gerasimova ³ , Sergey M. Zharkov ^{2,3} , Yaw-Teng Tseng ¹, Nicolay P. Shestakov ² and Irina S. Edelman ²

¹ Department of Applied Physics, National Pingtung University, Pingtung City 90003, Taiwan; stp92065@gmail.com (Y.-Z.C.); chargedw@yahoo.com.tw (Y.-T.T.)

² Kirensky Institute of Physics, FRC KSC SB RAS, 660036 Krasnoyarsk, Russia; irbiz@iph.krasn.ru (D.A.P.); alexeys@iph.krasn.ru (A.E.S.); zharkov@iph.krasn.ru (S.M.Z.); nico@iph.krasn.ru (N.P.S.); ise@iph.krasn.ru (I.S.E.)

³ Institute of Engineering Physics and Radio Electronics, Siberian Federal University, 660041 Krasnoyarsk, Russia; marina_2506@mail.ru

* Correspondence: crlinspin@gmail.com (C.-R.L.); osi@iph.krasn.ru (O.S.I.)

Abstract: Fe₃O₄@SiO₂ core-shell nanoparticles (NPs) were synthesized with the co-precipitation method and functionalized with NH₂ amino-groups. The nanoparticles were characterized by X-ray, FT-IR spectroscopy, transmission electron microscopy, selected area electron diffraction, and vibrating sample magnetometry. The magnetic core of all the nanoparticles was shown to be nanocrystalline with the crystal parameters corresponding only to the Fe₃O₄ phase covered with a homogeneous amorphous silica (SiO₂) shell of about 6 nm in thickness. The FT-IR spectra confirmed the appearance of chemical bonds at amino functionalization. The magnetic measurements revealed unusually high saturation magnetization of the initial Fe₃O₄ nanoparticles, which was presumably associated with the deviations in the Fe ion distribution between the tetrahedral and octahedral positions in the nanocrystals as compared to the bulk stoichiometric magnetite. The fluorescent spectrum of eosin Y-doped NPs dispersed in water solution was obtained and a red shift and line broadening (in comparison with the dye molecules being free in water) were revealed and explained. Most attention was paid to the adsorption properties of the nanoparticles with respect to three dyes: methylene blue, Congo red, and eosin Y. The kinetic data showed that the adsorption processes were associated with the pseudo-second order mechanism for all three dyes. The equilibrium data were more compatible with the Langmuir isotherm and the maximum adsorption capacity was reached for Congo red.

Keywords: Fe₃O₄@SiO₂; core-shell nanoparticles; magnetic properties; water pollutions; fluorescence; adsorption



Citation: Lin, C.-R.; Ivanova, O.S.; Petrov, D.A.; Sokolov, A.E.; Chen, Y.-Z.; Gerasimova, M.A.; Zharkov, S.M.; Tseng, Y.-T.; Shestakov, N.P.; Edelman, I.S. Amino-Functionalized Fe₃O₄@SiO₂ Core-Shell Magnetic Nanoparticles for Dye Adsorption. *Nanomaterials* **2021**, *11*, 2371. <https://doi.org/10.3390/nano11092371>

Academic Editor: Efrat Lifshitz

Received: 22 August 2021

Accepted: 9 September 2021

Published: 12 September 2021

Publisher's Note: MDPI stays neutral with regard to jurisdictional claims in published maps and institutional affiliations.



Copyright: © 2021 by the authors. Licensee MDPI, Basel, Switzerland. This article is an open access article distributed under the terms and conditions of the Creative Commons Attribution (CC BY) license (<https://creativecommons.org/licenses/by/4.0/>).

1. Introduction

Silica (SiO₂) is frequently used as a support-material in core-shell structures; it does not only help nanoparticles (NPs) to become stable at certain conditions, but also provides them an opportunity to be easily modified with other functional groups and, additionally, to be environmentally compatible. Furthermore, silica coated magnetic NPs can be dispersed in water without adding other surfactants due to the negative charges on the silica shells. The fields of application of Fe₃O₄@SiO₂ NPs functionalized with different surfactants, and more frequently with amines, are different. A number of authors have demonstrated their effective applications in biology and medicine [1,2], in catalysis [3,4], and, especially, as effective adsorbents for the removal of pollutants from wastewaters [5–12]. In ref. [1], the amino modifications of the silica surface of Fe₃O₄@SiO₂ NPs reduced the detrimental interactions with cellular membranes and prolonged the blood circulation time after in vivo administration. In ref. [12], the magnetic core-shell Fe₃O₄@SiO₂ NPs synthesized by the

modified Stöber method and functionalized with amino and carboxyl groups were used as a nano-adsorbent for scandium ions from aqueous solutions. In refs. [7,9], the synthesized $\text{Fe}_3\text{O}_4@\text{SiO}_2\text{-NH}_2$ nanocomposites were embedded into the polyether-sulfone membranes with different concentrations via the phase inversion method. Due to the nanocomposite adsorption properties, the significant enhancement in efficiency of the modified membranes for the removal of Cd(II) ions and methyl red dye was achieved. A new type of magnetic fluorescent nanocomposite ($\text{Fe}_3\text{O}_4@\text{SiO}_2\text{-NH}_2/\text{CQDs}$) was prepared by bonding of carbon quantum dots (CQDs) with $\text{Fe}_3\text{O}_4@\text{SiO}_2\text{-NH}_2$ nanocomposites through amine-carbonyl interactions and used as a fluorescent probe to detect Cu^{2+} [13]. The authors of ref. [11] concluded that the strategy of coating with silica and amino group functionalization of Fe_3O_4 nanoparticles is useful for increasing the adsorption capacity. In particular, they obtained adsorption capacities of 29.3 and 28.6 mg/g for light green and brilliant yellow anionic dyes, respectively, using $\text{Fe}_3\text{O}_4@\text{SiO}_2\text{-NH}_2$ NPs, while 12.1 and 9.4 mg/g only for Fe_3O_4 NPs. Since this line of research is rather new, and the properties and application possibilities of NPs strongly depend on the details of their synthesis, the search for optimal synthesis conditions and the study of the properties of the functionalized particles by various methods can be considered as an urgent task.

The present work is devoted to the study of the morphology, magnetic and adsorption properties of Fe_3O_4 NPs obtained by the co-precipitation method and then coated with amorphous silica to produce $\text{Fe}_3\text{O}_4@\text{SiO}_2$ core-shell NPs, which was functionalized by an amine group to fabricate $\text{Fe}_3\text{O}_4@\text{SiO}_2\text{-NH}_2$ nanocomposites. The methylene blue (MB), Congo red (CR) and eosin Y (EY) were selected as the typical organic cation and anion pollutants to test the ability of the prepared composite for the adsorptive removal of organic pollutants from water. The study of the fluorescent properties of eosin Y-doped NPs was also carried out.

2. Materials and Methods

2.1. Synthesis Procedure

Ferrous sulfate heptahydrate ($\text{FeSO}_4 \cdot 7\text{H}_2\text{O}$) (>99%) was obtained from Sigma-Aldrich, ethanol ($\text{CH}_3\text{CH}_2\text{OH}$) (>95%) was obtained from Fullin Nihon Shiyaku Biochemical Ltd., tetraethyl orthosilicate ($\text{Si}(\text{OC}_2\text{H}_5)_4$, TEOS) (>99%) and ammonia solution (28–30 wt.% NH_3) were purchased from Acros Organics. Potassium nitrate (KNO_3) (>99%) was purchased from Wako Pure Chemical Industries, Ltd. Sodium hydroxide pellets was obtained from PanReac AppliChem. Poly(sodium 4-styrene-sulfonate) solution (30 wt.%) in water was purchased from Aldrich. All the chemicals were used without further purification. Several stages were used to synthesize nanocomposites.

Magnetic NPs, Fe_3O_4 , were produced by co-precipitation, hydrolysis of iron sulfate under Ar flow. In the typical synthesis, a mixture of the basic solution is 0.02 mol KNO_3 and 0.2 mol NaOH in 50 mL of ultrapure water, previously deoxygenated, was prepared under Ar and, then was added dropwise to the Fe (II) solution (one is 0.25 M, the other is 0.75 M, and mixed together), under Ar and at 90 °C. The black precipitate formed was stirred over 1 h at 90 °C, then, washed thoroughly with ethanol. Silica coating of the magnetite nanoparticles was performed via the Stöber process. First, Fe_3O_4 NPs (200 mg) were dispersed in ethanol (150 mL) and kept immersed in a water bath over 15 min under sonication. Then, an ammonia solution (6 mL) and TEOS (200 μL) were slowly added to the Fe_3O_4 suspension. Finally, the SiO_2 coated particles were collected magnetically using an NdFeB magnet, and the isolated powders were washed thoroughly with ethanol (sample $\text{Fe}_3\text{O}_4@\text{SiO}_2$). The amino functionalization of silica coated NPs was made in the same manner as is mentioned above, replacing TEOS to (3-aminopropyl)-triethoxysilane (APTES) (sample $\text{Fe}_3\text{O}_4@\text{SiO}_2\text{-NH}_2$). At last, eosin Y was attached to the amino silanized magnetic nanoparticles covalently. First, $\text{Fe}_3\text{O}_4@\text{SiO}_2\text{-NH}_2$ NPs (200 mg) were dispersed in ultrapure water (50 mL) and over 15 min were exposed to sonication. The 0.2 mmol eosin Y and catalyst were added to the NPs suspension under stirring during 1 h, then, washed thoroughly with ethanol (sample $\text{Fe}_3\text{O}_4@\text{SiO}_2\text{-NH}_2\text{-EY}$).

2.2. Characteristic Methods

The crystal structure of the NPs was characterized by X-ray diffraction measurements using a Bruker D8 Advance diffractometer (Cu K α radiation, 40 kV, 25 mA, $\lambda = 1.5418 \text{ \AA}$) (Bruker Optik GmbH, Ettlingen, Germany).

The morphology and microstructure of the NPs were investigated using transmission electron microscopy (TEM). TEM experiments were performed with a JEM-2100 (JEOL Ltd., Tokyo, Japan) microscope operating at the accelerating voltage of 200 kV (Siberian Federal University) and JEOL JEM-1230 microscope (JEOL Ltd., Tokyo, Japan) operated at an accelerating voltage of 80 kV (Precision Instruments Center of NPUST). Selected-area electron diffraction (SAED) was used to determine the structure of the NPs.

Fourier transform infrared absorption (FT-IR) spectra were recorded with a VERTEX 70 (Bruker Optik GmbH, Ettlingen, Germany) spectrometer in the spectral region of $400 \div 4000 \text{ cm}^{-1}$ with the resolution 4 cm^{-1} . The spectrometer was equipped with a Globar as the light source and a wide band KBr beam splitter and RT-DLaTG as the detector (Bruker Optik GmbH). For the measurements, round tablet samples of about 0.5 mm thick and of 13 mm in diameter containing NPs were prepared as follows: nanopowders in amount lower than 0.001 g were thoroughly ground with 0.14 g of KBr; the mixtures were formed into tablets which were subjected to cold pressing at 10,000 kg.

The magnetic properties were measured with the vibrating sample magnetometer Lakeshore 7400 series VSM (Lake Shore Cryotronics, Inc., Westerville, OH, USA).

The excitation and fluorescence spectra were measured on a Fluorolog 3-22 spectrofluorometer (Horiba Jobin Yvon, Edison, NJ, USA). The obtained spectra were corrected for sensitivity of PMT, reabsorption effects and background. The quartz cells with the cross sections of $10 \times 10 \text{ mm}^2$ were used to investigate the solutions for L-geometry of excitation. All the measurements were carried out at room temperature.

The absorption spectra were recorded with a UV/VIS circular dichroism spectrometer SKD-2MUF (OEP ISAN, Moscow, Russia). Quartz cells with the optical path length of 5 mm were used.

3. Results and Discussion

3.1. NPs Structure and Morphology

The XRD patterns (Figure 1) revealed that the parent NPs and magnetic cores of all the nanocomposites were of the spinel ferrite crystal structure with the parameters of the most intense peaks corresponding to the Fe_3O_4 phase (PDF Card # 04-005-4319).

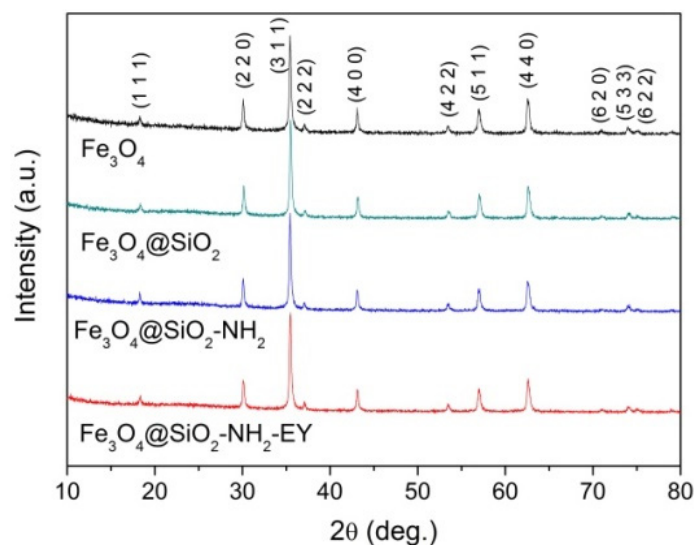


Figure 1. XRD patterns of synthesized NPs. The reflexes corresponding to PDF Card # 04-005-4319 are indicated in parenthesis.

The TEM images (Figure 2a–d) revealed NPs of predominantly rectangular shape with the average size of 25 ± 5 nm (Figure 2e). At the same time, a small amount of ellipsoidal NPs with the sizes of about 10 nm and rectangular NPs of a larger size can be noticed. The almost ideal crystal structure of the initial Fe_3O_4 NPs is seen very well in the HRTEM image in Figure 3a. As a result of the silica coating, the initial NPs became covered with a homogeneous amorphous silica shell, 6–7 nm thick seen especially well in the HRTEM image (Figure 3b). Functionalization with NH_2 and further doping with eosin Y led to some blurring of the HRTEM image (Figure 3c,d). The selected area electron diffraction (SAED) patterns also shown in Figure 3c,d confirm the presence of the Fe_3O_4 crystalline core in all NPs.

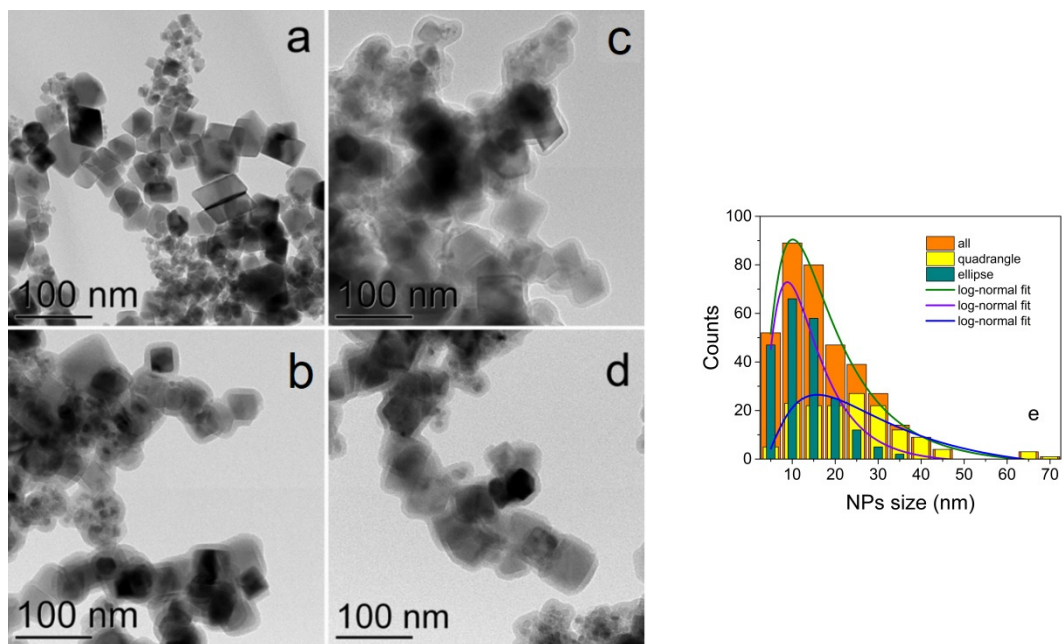


Figure 2. TEM images of Fe_3O_4 (a), $\text{Fe}_3\text{O}_4@SiO_2$ (b), $\text{Fe}_3\text{O}_4@SiO_2-NH_2$ (c) and $\text{Fe}_3\text{O}_4@SiO_2-NH_2-EY$ (d) NPs. Size distribution of Fe_3O_4 NPs (e).

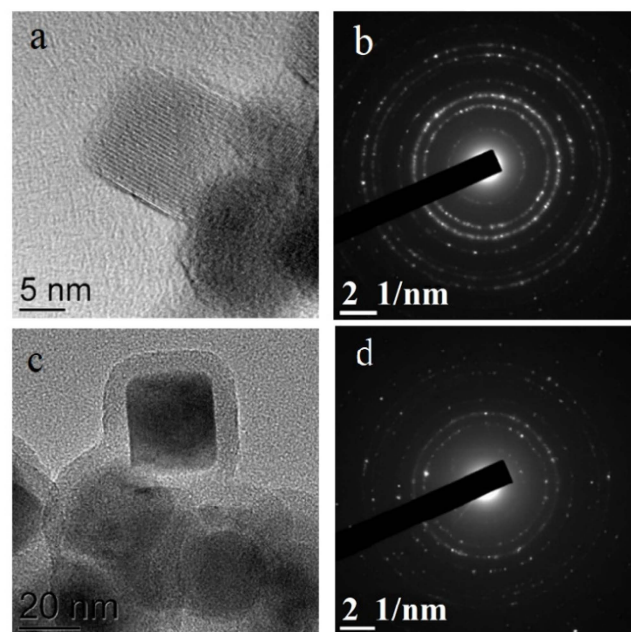


Figure 3. HRTEM image and selected area electron diffraction (SAED) of Fe_3O_4 (a,b) and $\text{Fe}_3\text{O}_4@SiO_2-NH_2$ (c,d) NPs, respectively.

The FT-IR spectra (Figure 4) show the appearance of new bands upon the transition $\text{Fe}_3\text{O}_4 \rightarrow \text{Fe}_3\text{O}_4@\text{SiO}_2 \rightarrow \text{Fe}_3\text{O}_4@\text{SiO}_2\text{-NH}_2 \rightarrow \text{Fe}_3\text{O}_4@\text{SiO}_2\text{-NH}_2\text{-EY}$ evidencing the appearance of chemical bonds. In the spectrum of pure Fe_3O_4 NPs, the strong band at 580 cm^{-1} is due to Fe-O stretching vibrations in accordance with other authors [9,11,13]. This band is observed in the spectra of all the samples. The wide asymmetric band at 1094 cm^{-1} appeared in the spectrum of the $\text{Fe}_3\text{O}_4@\text{SiO}_2$ sample and is seen in the spectra of two next samples having a SiO_2 shell. This band can be related to the asymmetric stretching vibrations of Si-O-Si. An analogous band was observed and interpreted equally by all the authors studying $\text{Fe}_3\text{O}_4@\text{SiO}_2$ NPs [9,11,13]. Symmetric Si-O-Si stretching vibrations were associated in [9] with the weak band near 808 cm^{-1} . The same weak band is seen at 800 cm^{-1} in Figure 4. At the same time, the authors of ref. [13] associated the band at 797 cm^{-1} with the Si-O-Fe stretching vibrations proving the presence of a chemical bond between the magnetic core and silica shell [9]. Only minor changes appear in the spectra of the $\text{Fe}_3\text{O}_4@\text{SiO}_2\text{-NH}_2$ and $\text{Fe}_3\text{O}_4@\text{SiO}_2\text{-NH}_2\text{-EY}$ samples. The appearance of a wide band near 3430 cm^{-1} is a more noticeable feature characteristic of the NH_2 amino group [14]. A small amount of covalently attached eosin Y in comparison with $\text{Fe}_3\text{O}_4@\text{SiO}_2\text{-NH}_2$ NPs does not allow one to clearly see changes in the bending and stretching vibrations of the amino groups.

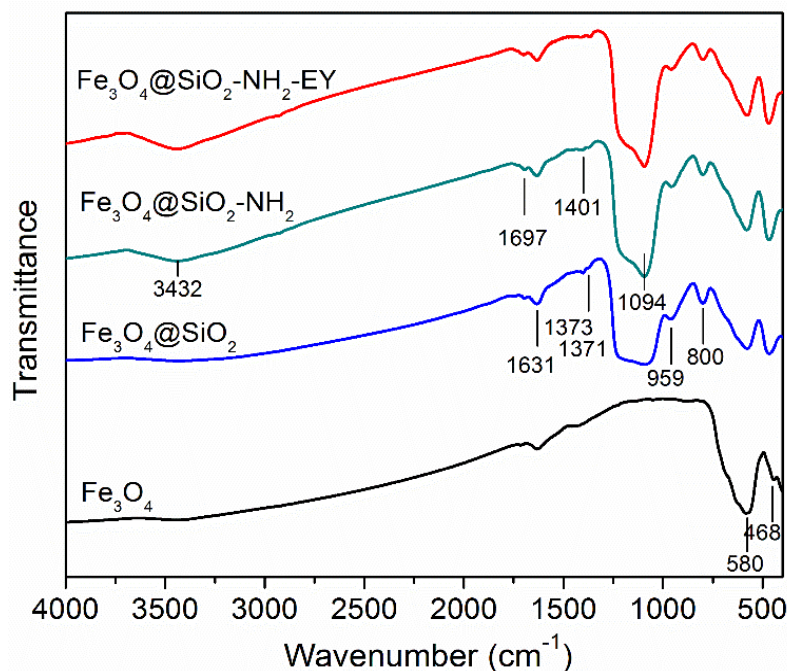


Figure 4. FT-IR spectra for Fe_3O_4 , $\text{Fe}_3\text{O}_4@\text{SiO}_2$, $\text{Fe}_3\text{O}_4@\text{SiO}_2\text{-NH}_2$, and $\text{Fe}_3\text{O}_4@\text{SiO}_2\text{-NH}_2\text{-EY}$.

3.2. NPs Magnetic Properties

The magnetic measurements (Figure 5) show very narrow hysteresis loops with magnetic saturation in the external magnetic field near 3 kOe and coercive force of about 100 Oe. The saturation magnetization M_s value of the initial Fe_3O_4 NPs is exceptionally high, significantly higher than the one presented by other authors for Fe_3O_4 NPs, for example [11] and even higher than in bulk Fe_3O_4 samples, 92 emu/g at room temperature [15]. The redistribution of Fe ions between the oppositely magnetized tetrahedral and octahedral sublattices in magnetite NPs caused, for example, by the technological conditions can be one of the reasons of the observed M_s increase. Since the resulting magnetization of the sample is due to the difference between the magnetic moments of Fe ions occupying octahedral and tetrahedral positions, the Fe ion deficiency in tetrahedral position can be responsible for an increase of the sample magnetization.

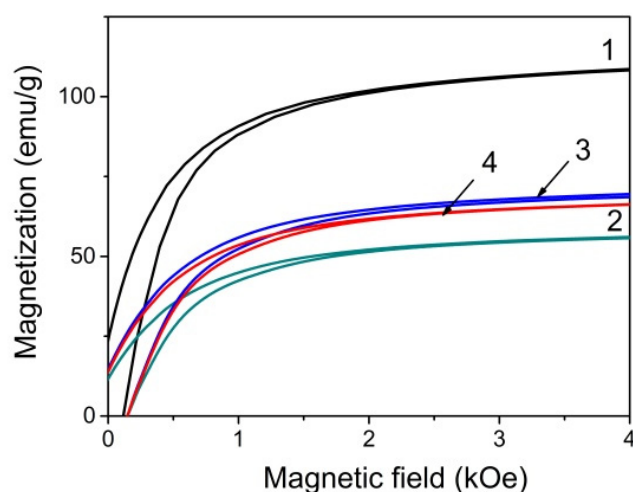


Figure 5. Room temperature magnetization curves for all NPs: Fe₃O₄ (1), Fe₃O₄@SiO₂ (2), Fe₃O₄@SiO₂-NH₂ (3), and Fe₃O₄@SiO₂-NH₂-EY (4).

The surface modifications lead to the M_s decrease. However, it remains quite high. A similar decrease in the saturation magnetization of Fe₃O₄ NPs coated with silica compared to the initial Fe₃O₄ nanoparticles was noted by a number of authors. For example, in ref. [11] M_s was equal to 38, 23, and 11 emu/g for Fe₃O₄, Fe₃O₄@SiO₂ and Fe₃O₄@SiO₂@NH₂ NPs, correspondingly; in ref. [16]—80, 31 and 20 emu/g for Fe₃O₄, Fe₃O₄@SiO₂ and Fe₃O₄@SiO₂-NH₂ NPs respectively.

The decrease in magnetization of NPs after coating with silicon oxide (curve 2 in Figure 5) can be caused by a number of factors. First of all, when determining the magnetization value, the whole particle mass was taken into account including the silica shell. In addition, the shell can affect the spin state of the magnetic core surface layers. However, the addition of the amino groups and then eosin Y resulted in an increase in magnetization. Such a behavior of the magnetization was not previously observed in the above-cited and other works. It is possible that, in the process of amino functionalization, cation redistribution between the sublattices continued. This question needs special consideration.

3.3. Application of Synthesized NPs as Fluorescent Probes

The development of hybrid nanoparticle technology, synthesized fluorescent nanoparticles with encapsulated quantum dots [17], or dyes [18] have attracted great interest in recent years. Despite the excellent brightness and photostability of quantum dots for imaging applications, the risk of systemic toxicity remains high due to the incorporation of heavy metals. Thus, dye-doped nanoparticles still appear very promising. The simultaneous combination of fluorescent and magnetic properties of NP imaging would greatly benefit in the diagnostics and monitoring of living cells and organisms [19,20].

The spectral properties of the synthesized EY-doped Fe₃O₄@SiO₂@NH₂ dispersed in water solution are presented in Figure 6a. The fluorescence spectrum turned out to be independent of the excitation wavelength and NPs give the green emission with the maximum at 542 nm with the excitation maximum at 515 nm. The fluorescent spectrum of EY-doped NPs dispersed in solution displays a red shift of 6 nm and 40 % broadening as compared with the dye molecules free in water in Figure 6b. On the contrary, the maximum of the excitation spectrum (measured at 580 nm) shows a slight blue shift of 1 nm and 30% broadening. The reasons for the observed spectral changes could include the change in the ionic form of the EY molecules and polarity decrease in the microenvironment. In the water solution, pH 6, most of the EY molecules are in the dianionic form. When attached to the amino groups in NPs, the dye changes its ionic form to the anionic or even neutral one and the spectral properties of these forms are different, on the one hand [21]. On other hand, as the solvent polarity decreases, the red shift in the emission of EY is observed [22].

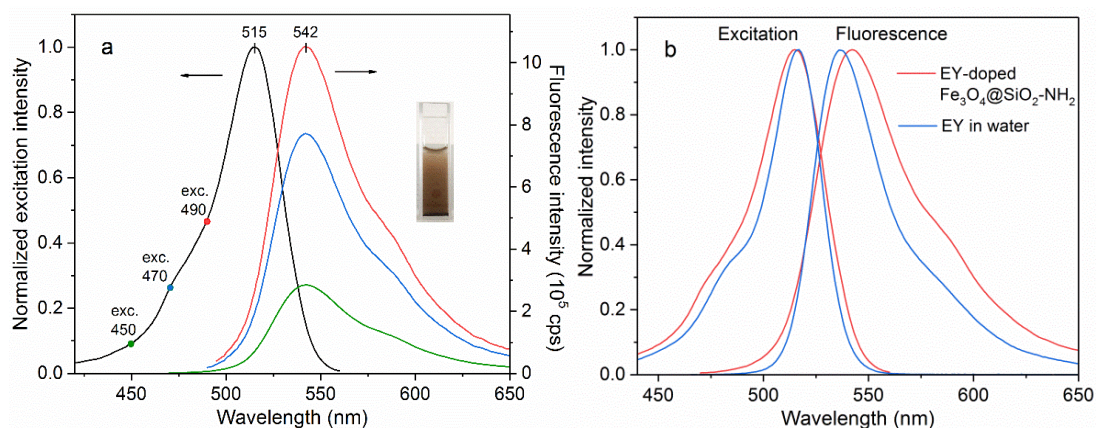


Figure 6. (a) Excitation spectrum and fluorescence spectrum of EY-doped $\text{Fe}_3\text{O}_4@\text{SiO}_2@\text{NH}_2$ dispersed in water under different excitation wavelengths. (b) Spectral changes of EY-doped NPs in comparison with EY free in distilled water (measured pH 5.5).

3.4. Application of Synthesized NPs for Dye Adsorption

3.4.1. Adsorption Kinetics

The spectral properties of two anionic (eosin Y (EY) and Congo red (CR)), and one cationic) methylene blue (MB) dyes were used to find out the adsorption capacity of amino-functionalized $\text{Fe}_3\text{O}_4@\text{SiO}_2$ core-shell magnetic NPs in distilled water (measured pH 5.5) at 25 °C. The dye concentration was determined by absorbance at the wavelength corresponding to the maxima in the spectra of 490 nm for eosin Y, 505 nm for CR, and 664 nm for MB.

For a typical experiment shown schematically in Figure 7, 3 mg of adsorbent was dispersed in 1.5 mL of the dye aqueous solution at the initial concentration of the dye $C_0 = 30$ mg/L. The solution was placed in an ultrasonic bath for 10 min for intensive mixing. Then, a magnetic nanoadsorbent was separated from the solution by applying a magnetic field and the absorption spectra of the solution were measured. The shaking and magnetic separation was repeated multiple times to obtain kinetic curves. The value of the adsorption capacity q_t (mg/g) of NPs was calculated as follows

$$q_t = \frac{(C_0 - C_t)V}{m}, \quad (1)$$

where C_0 and C_t (mg/L) are the initial concentration and concentration of the dye at the contact time t , V (L) is the volume of the solution; and m (g) is the mass of the adsorbent (NPs).

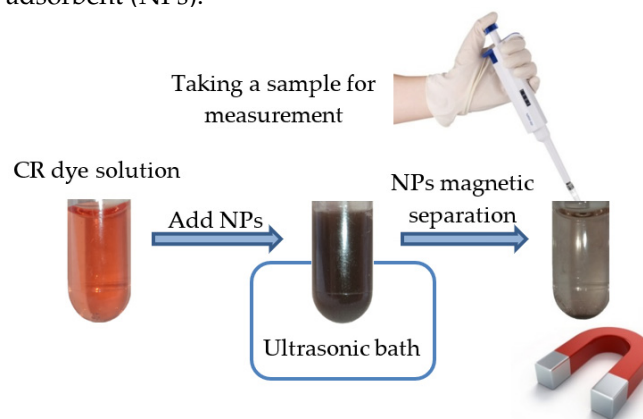


Figure 7. Schematic picture showing the preparation of a sample to measure the adsorption capacity, using the CR ($C_0 = 30$ mg/L) water solution as an example.

The effect of the contact time on the adsorption of $\text{Fe}_3\text{O}_4@\text{SiO}_2\text{-NH}_2$ NPs is shown in Figure 8 for the dyes at the same initial concentration of $C_0 = 30$ mg/L. At the initial stage of adsorption kinetics, the amount of the adsorbed dye onto the magnetic NPs increases rapidly due to a large number of vacant active sites on the surface of the amino-functionalized silica coated magnetic NPs. After that, these surface sites are gradually occupied, so the adsorption rate decreases until the adsorption equilibrium is established. The time to reach the equilibrium adsorption for the anionic dyes on $\text{Fe}_3\text{O}_4@\text{SiO}_2\text{-NH}_2$ NPs is much faster than for the cationic dye: 60 min for EY, 100 min for CR, and more than 300 min for MB. The other adsorbent $\text{Fe}_3\text{O}_4@\text{SiO}_2@\text{NH}_2@\text{Zn-TDPA}$ NPs [TDPAT = 2,4,6-tris(3,5-dicarboxyl phenylamino)-1,3,5-triazine] showed the similar time of 120 min both for the cationic MB and anionic CR dye [23]. The adsorption of CR by the $\text{Fe}_3\text{O}_4@\text{SiO}_2$ nanospheres achieved the equilibrium only after 5 h [24]. The equilibrium adsorption for initial concentration of $C_0 = 30$ mg/L was measured after 24 h of contact of NPs with the dye solution. The equilibrium adsorption capacity q_e of CR (11.6 mg/g) is higher than that of EY (7.2 mg/g) and MB (9.8 mg/g).

A quantitative understanding of the adsorption is possible with the help of kinetic models. The adsorption kinetics of the dyes on the magnetic NPs was described by the kinetic models of the pseudo-first order:

$$\ln(q_e - q_t) = \ln q_e - k_1 t \quad (2)$$

and of the pseudo-second order:

$$\frac{t}{q_t} = \frac{1}{k_2 q_e^2} + \frac{t}{q_e} \quad (3)$$

where q_e and q_t (mg/g) are the amounts of the dye at equilibrium and at contact time t , respectively; k_1 (1/min) and k_2 (g/(mg min)) are the adsorption rate constants of the reaction of the pseudo-first and pseudo-second orders, respectively.

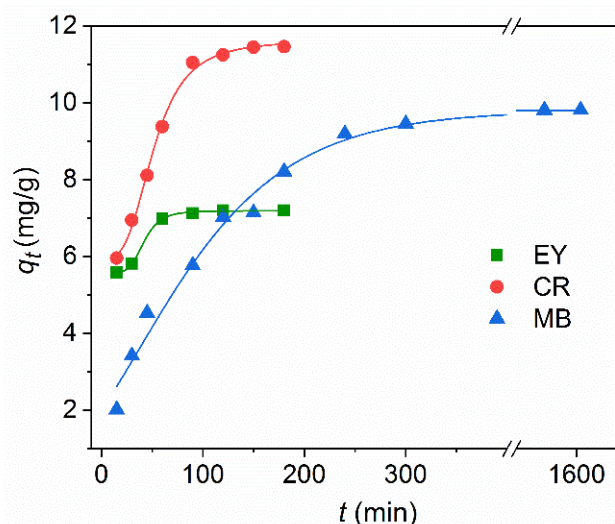


Figure 8. The effect of contact time on the dye adsorption for $\text{Fe}_3\text{O}_4@\text{SiO}_2@\text{NH}_2$ NPs at 25 °C. Experimental conditions: $C_0 = 30$ mg/L, $m(\text{NPs}) = 3$ mg in $V = 1.5$ mL.

The curve-fitting plots of the adsorption ability of the dyes by $\text{Fe}_3\text{O}_4@\text{SiO}_2\text{-NH}_2$ NPs using the two kinetic models are shown in Figure 9, and the fitted parameters with the correlation coefficients R^2 are summarized in Table 1. The R^2 values for the pseudo-second order kinetic model ($R^2 = 0.995\text{--}0.999$) were higher than those of the pseudo-first order model ($R^2 = 0.903\text{--}0.970$). In addition, the calculated values of q_e (Table 1) determined by the pseudo-second order model are more consistent with the measured values of q_e than that of the pseudo-first-order model. These results prove that the adsorption process of these

dyes on Fe₃O₄@SiO₂-NH₂ NPs completely followed a the pseudo-second order kinetic model, suggesting that adsorption is dependent on the amount of the solute adsorbed on the surface of the adsorbent and the amount of active sites. It should be noted that the dye adsorption kinetics on magnetic nanoparticles is most often described in terms of the pseudo-second order model [23–30].

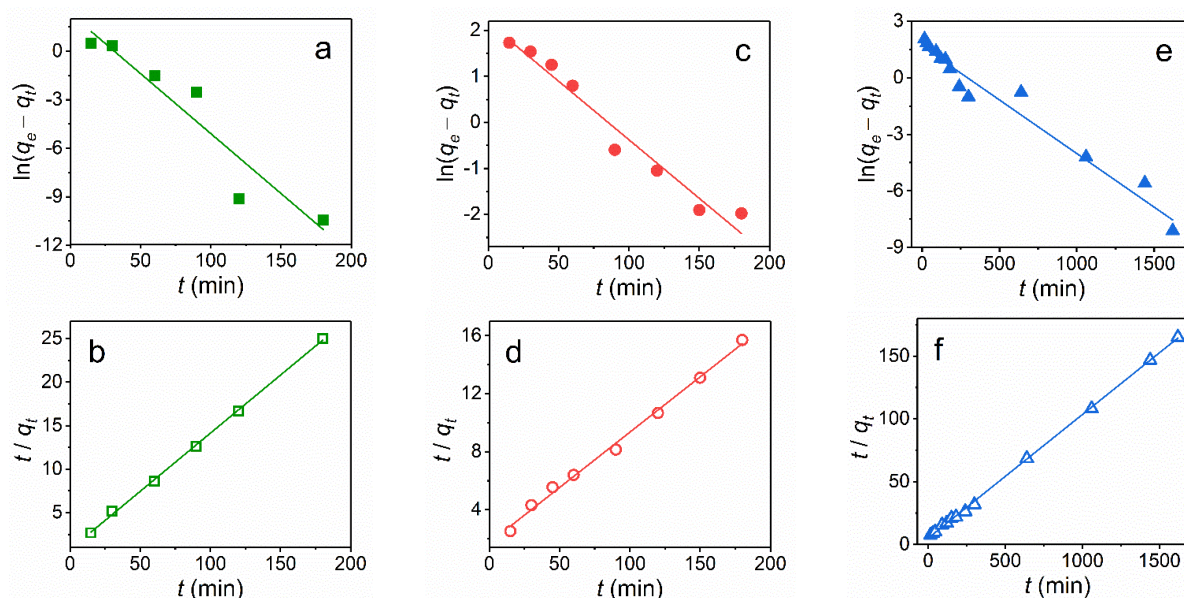


Figure 9. The pseudo-first-order (a,c,e) and pseudo-second-order (b,d,f) kinetics of EY (a,b), CR (c,d) and MB (e,f) adsorption on amino-functionalized Fe₃O₄@SiO₂ core-shell magnetic NPs at 25 °C.

Table 1. Kinetic parameters (Equations (2)–(4)) for the adsorption of the dyes (initial C₀ = 30 mg/L) on Fe₃O₄@SiO₂-NH₂ NPs at 25 °C.

Kinetics	Parameters	EY	CR	MB
Pseudo-first order model	k_1 (1/min)	0.074 ± 0.012	0.025 ± 0.002	0.0057 ± 0.0003
	q_e (mg/g)	10.2 ± 3.4	8.7 ± 1.4	5.3 ± 1.2
	R^2	0.903	0.964	0.970
Pseudo-second order model	k_2 (g/(mg min))	0.023 ± 0.005	0.0034 ± 0.0005	0.0019 ± 0.0002
	q_e (mg/g)	7.5 ± 0.6	12.6 ± 0.9	10.2 ± 0.8
	R^2	0.999	0.995	0.999
Intraparticle diffusion model	k_{i1} (mg/(g min ^{0.5}))	0.37 ± 0.07	0.93 ± 0.06	0.60 ± 0.03
	C_1 (mg/g)	4.0 ± 0.6	2.1 ± 0.3	0.11 ± 0.03
	R^2	0.938	0.988	0.986
	k_{i2} (mg/g min ^{0.5})	0.04 ± 0.01	0.11 ± 0.02	0.024 ± 0.006
	C_2 (mg/g)	6.7 ± 0.2	10.0 ± 0.3	8.9 ± 0.2
	R^2	0.873	0.929	0.902

The intraparticle diffusion model is often used to identify diffusion mechanisms [23,25–28,30,31]. In this model, the rate of intraparticle diffusion is a function of $t^{0.5}$ and can be determined as follows:

$$q_t = k_i t^{0.5} + C, \quad (4)$$

where k_i is the intraparticle diffusion rate constant, (mg/g.min^{0.5}). C is the intercept of the linear curve. According to the model proposed by Weber and Morris [32], the adsorption process is controlled only by intraparticle diffusion if the plot is a straight line and passes

through the origin. Otherwise, if the plot is multilinear or does not pass the origin, more than one diffusion mechanism might determine the adsorption process and adsorption is related to diffusion within the particles.

As shown in Figure 10, at least two stages are observed for anionic CR, EY as well as for the cationic MB dye, and thus, two or more diffusion mechanisms can affect the adsorption. The first stage refers to the transport of the dye molecules from the solution to the external surface of NPs. This stage is completed after up to 60 min for EY, 90 min for CR, and 240 min for MB. The second stage corresponds to the diffusion of the dye molecules within the micropores of $\text{Fe}_3\text{O}_4@\text{SiO}_2\text{-NH}_2$ NPs. The high initial absorption rates k_{i1} of the first stage (Table 1) are observed for all the dyes, indicating a fast initial dye removal process and the predominant role of external surface diffusion, especially, for CR. Extremely low adsorption rates k_{i2} (8–25 fold less than for the first stage) shows a negligible proportion of intraparticle diffusion of the dye molecules within the micropores of NPs. A similar two-stage adsorption process was observed for MB onto B- $\text{Fe}_3\text{O}_4@\text{C}$ NPs [28], for CR and MB dyes onto $\text{Fe}_3\text{O}_4@\text{SiO}_2@\text{NH}_2@\text{Zn-TDPA}$ NPs [23], and for EY onto $\text{Fe}_3\text{O}_4/\text{polypyrrole}$ composites [30].

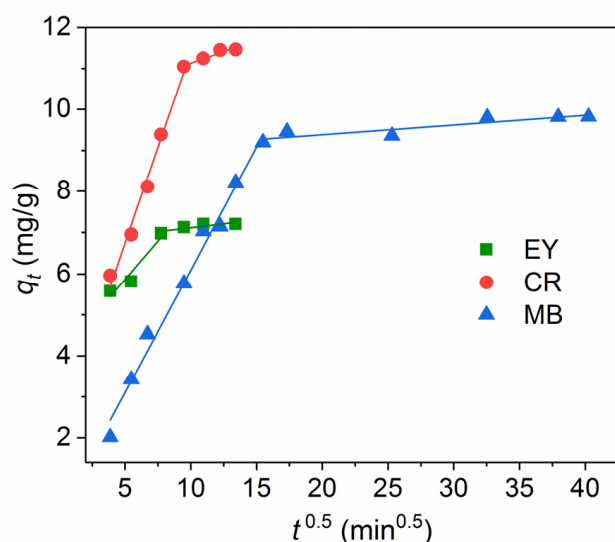


Figure 10. Intraparticle diffusion kinetic model of the dye adsorption on the amino-functionalized $\text{Fe}_3\text{O}_4@\text{SiO}_2$ core-shell magnetic NPs at 25 °C.

3.4.2. Adsorption Isotherms

Two adsorption isotherm models (Langmuir and Freundlich) were applied to understand the adsorbate–adsorbent interaction. The Langmuir equation was defined as follows

$$q_e = \frac{q_{\max} K_L C_e}{K_L C_e + 1}, \quad (5)$$

where q_e (mg/g) is the amount of the dye adsorbed at the equilibrium, q_{\max} represents the maximum adsorption capacity (mg/g), K_L is the Langmuir adsorption constant (L/mg), and C_e is the equilibrium concentration of the adsorbed dye (mg/L).

The Freundlich equation is expressed as:

$$q_e = K_F C_e^{1/n}, \quad (6)$$

where K_F is the Freundlich adsorption constant (L/mg); the dimensionless constant $1/n$ is an empirical parameter related to the isotherm shape. Based on the $1/n$ values, the adsorption process can be classified as irreversible ($1/n = 0$), favorable ($0 < 1/n < 1$), or unfavorable ($1/n > 1$) [33].

The Langmuir model illustrates the formation of a homogeneous adsorbed monolayer, while the adsorbed molecules do not interact with each other. The Freundlich model considers the existence of a more complicated multilayered structure.

Based on the results presented above, we have chosen the anionic CR dye for further investigation owing to its highest capacity and shortest time of the adsorption process. The adsorption isotherm models were used to describe the equilibrium between the adsorbed CR on the surface of $\text{Fe}_3\text{O}_4@\text{SiO}_2\text{-NH}_2$ NPs (Figure 11). The obtained parameters are presented in Table 2. According to the correlation coefficients, the Langmuir model ($R^2 = 0.967$) coincided with the experimental data much better than the Freundlich model ($R^2 = 0.789$), which indicates that the homogeneous and monolayer adsorption is the dominant adsorption in the case of CR. Although the $1/n$ value is lower than 1 and indicates that the adsorption of CR is favorable, the R^2 values of the Freundlich isotherm do not fall within the acceptable range. In contrast to our results, the adsorption isotherm of CR on $\text{Fe}_3\text{O}_4@\text{SiO}_2@\text{Zn-TDPAT}$ NPs was satisfactorily described both by the Langmuir and Freundlich models [23].

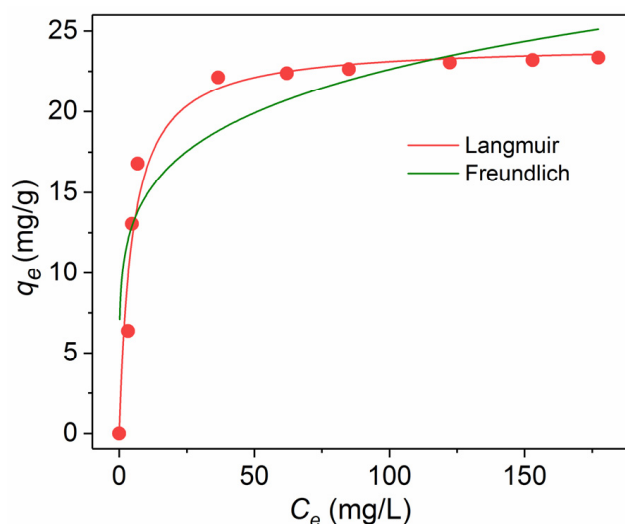


Figure 11. Adsorption isotherms of CR on magnetic NPs at 25 °C.

Table 2. Adsorption isotherm parameters (Equations (5) and (6)) for Congo red at 25 °C.

Langmuir Model			Freundlich Model		
q_{\max} , mg/g	K_L , L/mg	R^2	$1/n$	K_F , L/mg	R^2
24 ± 1	0.21 ± 0.04	0.967	0.18 ± 0.04	0.010 ± 0.002	0.789

The adsorbents based on $\text{Fe}_3\text{O}_4@\text{SiO}_2$ nanoparticles for the removal of the anionic CR and cationic MB dyes are summarized in Table 3. The maximum adsorption capacity q_{\max} of the synthesized amino-functionalized $\text{Fe}_3\text{O}_4@\text{SiO}_2$ core-shell magnetic nanoparticles is comparable to other analogous adsorbents [10,23,24,29,34].

As is seen from Table 3, the adsorption efficiency can further be improved by the surface modification of NPs. It should be emphasized that the pH and ionic strength of the aqueous solution [23] as well as the temperature [24] could also significantly influence the efficiency of the dye adsorption on NPs due to the involvement of different adsorption mechanisms including electrostatic and hydrophobic interactions, hydrogen bonding, van der Waals forces, etc. The measured zeta potential of the $\text{Fe}_3\text{O}_4@m\text{SiO}_2\text{-NH}_2$ nanoparticles vs. pH showed [35] that the isoelectric point was at 5.9 due to the amino-functionalization, denoting that the modified nanoparticles would be positively charged at $\text{pH} < 5.9$ and negatively charged at $\text{pH} > 5.9$. Under the conditions of our experiment (the initial pH 5.5), the surface of the magnetic NPs had a slightly positive charge. Table 3 indicates that the

maximum adsorption capacity q_{\max} is close for both anionic CR and cationic MB dyes, so the electrostatic interactions are not only responsible for the adsorption of the dyes on NPs.

Table 3. Comparison of the adsorption capacity of the $\text{Fe}_3\text{O}_4@SiO_2$ core-shell magnetic nanoparticles for the anionic CR and cationic MB dyes.

Anionic Dye	Adsorbent	q_{\max} (mg/g)	Cationic Dye	Adsorbent	q_{\max} (mg/g)
CR	$\text{Fe}_3\text{O}_4@SiO_2-NH_2$	24.0 [This work]	MB	$\text{Fe}_3\text{O}_4@SiO_2-NH_2$	20 ^a [This work]
	$\text{Fe}_3\text{O}_4@SiO_2-NH_2$	18.0 [29]		$\text{Fe}_3\text{O}_4@SiO_2$	31.8 [24]
	$\text{Fe}_3\text{O}_4@SiO_2-NH_2-MIP^b$	35.3 [29]		$\text{Fe}_3\text{O}_4@SiO_2$	32.3 [23]
	$\text{Fe}_3\text{O}_4@SiO_2$	36.2 [24]		$\text{Fe}_3\text{O}_4@SiO_2-CR^c$	31.4 [34]
	$\text{Fe}_3\text{O}_4@SiO_2$	14.8 [23]		$\text{Fe}_3\text{O}_4@SiO_2@Zn-TDPAT^d$	58.7 [23]
	$\text{Fe}_3\text{O}_4@SiO_2@Zn-TDPAT^d$	17.7 [23]		$\text{Fe}_3\text{O}_4@SiO_2-(CH_2)_3-IL/Talc^e$	6.2 [10]

^a $q_{\max} = q_e$ at $C_0 = 60$ mg/L. ^b MIP is the molecularly imprinted polymer. ^c CR is Congo red. ^d TDPAT is 2,4,6-tris(3,5-dicarboxyl phenylamino)-1,3,5-triazine. ^e IL is the ionic liquid.

4. Conclusions

In this study, core-shell magnetic nanoparticles, $\text{Fe}_3\text{O}_4@SiO_2$, were synthesized by silica coating of the initial Fe_3O_4 NPs via the Stöber process and then functionalized with amino groups NH_2 . X-ray and electron diffraction data showed the magnetic core of the particles to have the magnetite Fe_3O_4 crystal structure without the presence of any other phases. Transmission electron microscopy showed predominantly rectangular NPs with the average size of 25 ± 5 nm in the initial Fe_3O_4 powder sample. The homogeneous amorphous silica shells with the thickness of about 7 nm were formed around each initial NP. The FT-IR spectra confirmed the appearance of the chemical bonds between the silica shell and magnetic core of NPs as well between the silica and amino group. The magnetic measurements revealed unusually high saturation magnetization M_s of the initial Fe_3O_4 NPs even higher than this value of the bulk magnetite crystal. M_s of the functionalized samples also significantly exceeded M_s of similar samples presented in literature. The high M_s value can be considered as an advantage of the studied nanomaterials since higher magnetization requires the use of weaker magnetic fields to control the processes involving these materials.

The fluorescence spectrum of EY-doped $\text{Fe}_3\text{O}_4@SiO_2@NH_2$ NPs dispersed in water solution was studied. NPs gave the green emission with the maximum at 542 nm with the excitation maximum at 515 nm. The spectrum displayed a red shift of about 6 nm and 40% broadening as compared to the dye molecules free in water while the maximum of the excitation spectrum (measured at 580 nm) showed a slight blue shift of 1 nm and 30% broadening. The observed spectral changes were associated with the change in the ionic form of the EY molecules due to the attachment to the amino groups in NPs.

The dye adsorption capacity and kinetics of the amino-functionalized $\text{Fe}_3\text{O}_4@SiO_2$ core-shell magnetic NPs were studied in application to two anionic (eosin Y (EY) and Congo red (CR), and one cationic) methylene blue (MB) dyes. It was shown that the adsorption process of these dyes on the studied NPs followed the pseudo-second order kinetic model, suggesting that sorption is dependent on the amount of the solute adsorbed on the surface of the adsorbent and the amount of active sites. At least two stages were revealed in the adsorption time dependence for all three dyes. In the first stage, the transport of the dye molecules from the solution to the external surface of NPs occurs. The second stage corresponds to the diffusion of the dye molecules within the micropores of NPs. The high initial absorption rates of the first stage were observed for all the dyes, indicating a fast initial dye removal process and the predominant role of the external surface diffusion, especially, for CR. It was shown that the experimental data were fitted to the Langmuir model of the adsorption processes indicating that the homogeneous and monolayer adsorption was the dominant adsorption in the considered cases. The maximum adsorption capacity of

the synthesized amino-functionalized Fe₃O₄@SiO₂ core-shell magnetic nanoparticles is comparable to other analogous adsorbents presented in literature.

Author Contributions: Conceptualization, C.-R.L. and I.S.E.; data curation, O.S.I., A.E.S., and D.A.P.; formal analysis, M.A.G.; funding acquisition, C.-R.L. and I.S.E.; investigation, M.A.G., O.S.I., D.A.P., A.E.S., S.M.Z., Y.-Z.C., and N.P.S.; methodology, M.A.G., O.S.I., and S.M.Z., Y.-T.T.; project administration, C.-R.L. and I.S.E.; resources, A.E.S. and Y.-Z.C.; supervision, C.-R.L. and I.S.E.; validation, I.S.E.; visualization M.A.G., Y.-T.T., and O.S.I.; writing—original draft, I.S.E.; writing—review and editing, M.A.G. and I.S.E. All authors have read and agreed to the published version of the manuscript.

Funding: The authors are thankful for the financial support the Russian Foundation for Basic Research, Grant № 19-52-52002, Ministry of Science and Technology of Taiwan, Grants MOST № 108-2923-M-153-001-MY3 and № 109-2112-M-153-003-, the Russian Foundation for Basic Research with Government of Krasnoyarsk Territory, Krasnoyarsk Regional Fund of Science, the research project number 19-42-240005: “Features of the electronic structure, magnetic properties and optical excitations in nanocrystals of the multifunctional magnetic chalcogenides Fe₃S₄ and FeSe”. We thank also the SFU Joint Scientific Center supported by the State assignment (#FSRZ-2020-0011) of the Ministry of Science and Higher Education of the Russian Federation, where the Transmission Electron Microscopy studies were carried out.

Institutional Review Board Statement: The study was conducted according to the guidelines of the Declaration of Helsinki, and approved by the Institutional Review Board of Kirensky Institute of Physics (b/n 20.08.2021).

Informed Consent Statement: Informed consent was obtained from all subjects involved in the study.

Data Availability Statement: The data presented in this study are available on request from the corresponding author. The data are not publicly available since they are a part of ongoing research.

Conflicts of Interest: The authors declare no conflict of interest.

References

1. Li, J.; Yuan, Z.; Liu, H.; Feng, J.; Chen, Z. Size-dependent tissue-specific biological effects of core-shell structured Fe₃O₄@SiO₂-NH₂ nanoparticles. *J. Nanobiotechnol.* **2019**, *17*, 124. [[CrossRef](#)]
2. Aslani, E.; Abri, A.; Pazhang, M. Immobilization of trypsin onto Fe₃O₄@SiO₂-NH₂ and study of its activity and stability. *Colloids Surf. B Biointerfaces* **2018**, *170*, 553–562. [[CrossRef](#)]
3. Izgi, M.S.; Ece, M.Ş.; Kazici, H.Ç.; Şahin, Ö.; Onat, E. Hydrogen production by using Ru nanoparticle decorated with Fe₃O₄@SiO₂-NH₂ core-shell microspheres. *Int. J. Hydrog. Energy* **2020**, *45*, 30415–30430. [[CrossRef](#)]
4. Veisi, H.; Ozturk, T.; Karmakar, B.; Tamoradi, T.; Hemmati, S. In situ decorated Pd NPs on chitosan-encapsulated Fe₃O₄/SiO₂-NH₂ as magnetic catalyst in Suzuki-Miyaura coupling and 4-nitrophenol reduction. *Carbohydr. Polym.* **2020**, *235*, 115966. [[CrossRef](#)]
5. Salman, M.; Jahan, S.; Kanwal, S.; Mansoor, F. Recent advances in the application of silica nanostructures for highly improved water treatment: A review. *Environ. Sci. Pollut. Res.* **2019**, *26*, 21065–21084. [[CrossRef](#)] [[PubMed](#)]
6. Xie, H.; Wu, Z.; Wang, Z.; Lu, J.; Li, Y.; Cao, Y.; Cheng, H. Facile fabrication of acid-resistant and hydrophobic Fe₃O₄@SiO₂@C magnetic particles for valid oil-water separation application. *Surf. Interfaces* **2020**, *21*, 100651. [[CrossRef](#)]
7. Zhang, S.; Zhang, Y.; Liu, J.; Xu, Q.; Xiao, H.; Wang, X.; Xu, H.; Zhou, J. Thiol modified Fe₃O₄@SiO₂ as a robust, high effective, and recycling magnetic sorbent for mercury removal. *Chem. Eng. J.* **2013**, *226*, 30–38. [[CrossRef](#)]
8. Ghorbani, F.; Kamari, S. Core-shell magnetic nanocomposite of Fe₃O₄@SiO₂@NH₂ as an efficient and highly re-cyclable adsorbent of methyl red dye from aqueous environments. *Environ. Technol. Innov.* **2019**, *14*, 100333. [[CrossRef](#)]
9. Kamari, S.; Shahbazi, A. Biocompatible Fe₃O₄@SiO₂-NH₂ nanocomposite as a green nanofiller embedded in PES-nanofiltration membrane matrix for salts, heavy metal ion and dye removal: Long-term operation and re-usability tests. *Chemosphere* **2020**, *243*, 125282. [[CrossRef](#)]
10. Alizadeh, A.; Fakhari, M.; Safaei, Z.; Khodeai, M.; Repo, E.; Asadi, A. Ionic liquid-decorated Fe₃O₄@SiO₂ nanocomposite coated on talc sheets: An efficient adsorbent for methylene blue in aqueous solution. *Inorg. Chem. Commun.* **2020**, *121*, 108204. [[CrossRef](#)]
11. Erdem, B.; Avcı, S.B.; Erdem, S.; Tekin, N. Adsorption of light green and brilliant yellow anionic dyes using amino functionalized magnetic silica (Fe₃O₄@SiO₂@NH₂) nanocomposite. *J. Dispers. Sci. Technol.* **2018**, *40*, 1227–1235. [[CrossRef](#)]
12. Salman, A.D.; Juzsakova, T.; Ákos, R.; Ibrahim, R.I.; Al-Mayyahi, M.; Mohsen, S.; Abdullah, T.A.; Domokos, E. Synthesis and surface modification of magnetic Fe₃O₄@SiO₂ core-shell nanoparticles and its application in up-take of scandium (III) ions from aqueous media. *Environ. Sci. Pollut. Res.* **2021**, *28*, 28428–28443. [[CrossRef](#)]
13. Dong, S.; Wang, S.; Wang, X.; Zhai, L. Superparamagnetic nanocomposite Fe₃O₄@SiO₂-NH₂/CQDs as fluorescent probe for copper (II) detection. *Mater. Lett.* **2020**, *278*, 128404. [[CrossRef](#)]

14. Alenazi, N.A.; Hussein, M.A.; Alamry, K.A.; Asiri, A.M. Nanocomposite-Based Aminated Polyethersulfone and Carboxylate Activated Carbon for Environmental Application. A Real Sample Analysis. *C* **2018**, *4*, 30. [[CrossRef](#)]
15. Smit, J.; Wijn, H.P.J. *Ferrites: Physical Properties of Ferrimagnetic Oxides in Relation to their Technical Applications*; Philips Gloeilamp-fabrieken: Eindhoven, The Netherlands, 1959.
16. Mahdavi, M.; Ahmad, M.B.; Haron, M.J.; Gharayebi, Y.; Shameli, K.; Nadi, B. Fabrication and characterization of SiO₂/(3-aminopropyl) triethoxysilane-coated magnetite nanoparticles for lead(II) removal from aqueous solution. *J. Inorg. Organomet. Polym.* **2013**, *23*, 599–607. [[CrossRef](#)]
17. Rizvi, S.B.; Ghaderi, S.; Keshtgar, M.; Seifalian, A.M. Semiconductor quantum dots as fluorescent probes for in vitro and in vivo bio-molecular and cellular imaging. *Nano Rev.* **2010**, *1*, 5161. [[CrossRef](#)] [[PubMed](#)]
18. Zhang, W.-H.; Hu, X.-X.; Zhang, X.-B. Dye-doped fluorescent silica nanoparticles for live cell and in vivo bioimaging. *Nanomaterials* **2016**, *6*, 81. [[CrossRef](#)] [[PubMed](#)]
19. Chekina, N.; Horák, D.; Jendelova, P.; Trchova, M.; Beneš, M.J.; Hruby, M.; Herynek, V.; Turnovcová, K.; Syková, E. Fluorescent magnetic nanoparticles for biomedical applications. *J. Mater. Chem.* **2011**, *21*, 7630–7639. [[CrossRef](#)]
20. Heitsch, A.T.; Smith, D.K.; Patel, R.N.; Ress, D.; Korgel, B.A. Multifunctional particles: Magnetic nanocrystals and gold nanorods coated with fluorescent dye-doped silica shells. *J. Solid State Chem.* **2008**, *181*, 1590–1599. [[CrossRef](#)]
21. Slyusareva, E.A.; Gerasimova, M.A. pH-dependence of the absorption and fluorescent properties of fluorone dyes in aqueous solutions. *Russ. Phys. J.* **2014**, *56*, 1370–1377. [[CrossRef](#)]
22. Chakraborty, M.; Panda, A.K. Spectral behaviour of eosin y in different solvents and aqueous surfactant media. *Spectrochim. Acta A* **2011**, *82*, 458–465. [[CrossRef](#)] [[PubMed](#)]
23. Wo, R.; Li, Q.-L.; Zhu, C.; Zhang, Y.; Qiao, G.-F.; Lei, K.-Y.; Du, P.; Jiang, W. Preparation and Characterization of Functionalized Metal–Organic Frameworks with Core/Shell Magnetic Particles (Fe₃O₄@SiO₂@MOFs) for Removal of Congo Red and Methylene Blue from Water Solution. *J. Chem. Eng. Data* **2019**, *64*, 2455–2463. [[CrossRef](#)]
24. Wang, P.; Wang, X.; Yu, S.; Zou, Y.; Wang, J.; Chen, Z.; Alharbi, N.S.; Alsaedi, A.; Hayat, T.; Chen, Y.; et al. Silica coated Fe₃O₄ magnetic nanospheres for high removal of organic pollutants from wastewater. *Chem. Eng. J.* **2016**, *306*, 280–288. [[CrossRef](#)]
25. Hamed, A.; Trotta, F.; Zarandi, M.B.; Zanetti, M.; Caldera, F.; Anceschi, A.; Nateghi, M.R. In Situ Synthesis of MIL-100(Fe) at the Surface of Fe₃O₄@AC as Highly Efficient Dye Adsorbing Nanocomposite. *Int. J. Mol. Sci.* **2019**, *20*, 5612. [[CrossRef](#)]
26. Huang, P.; Xia, D.; Kazlauciusas, A.; Thornton, P.; Lin, L.; Menzel, R. Dye-mediated interactions in chitosan-based polyelectrolyte/organoclay hybrids for enhanced adsorption of industrial dyes. *ACS Appl. Mater. Interfaces* **2019**, *11*, 11961–11969. [[CrossRef](#)] [[PubMed](#)]
27. Gouamid, M.; Ouahrani, M.R.; Bensaci, M.B. Adsorption equilibrium, kinetics and thermodynamics of methylene blue from aqueous solutions using Date palm Leaves. *Energy Procedia* **2013**, *36*, 898–907. [[CrossRef](#)]
28. Qu, L.; Han, T.; Luo, Z.; Liu, C.; Mei, Y.; Zhu, T. One-step fabricated Fe₃O₄@C core–shell composites for dye removal: Kinetics, equilibrium and thermodynamics. *J. Phys. Chem. Solids* **2015**, *78*, 20–27. [[CrossRef](#)]
29. Harsini, N.N.; Ansari, M.; Kazemipour, M. Synthesis of Molecularly Imprinted Polymer on Magnetic Core-Shell Silica Nanoparticles for Recognition of Congo Red. *Eurasian J. Anal. Chem.* **2018**, *13*, 20. [[CrossRef](#)]
30. Zhang, M.; Yu, Z.; Yu, H. Adsorption of eosin Y, methyl orange and brilliant green from aqueous solution using ferroferric oxide/polypyrrole magnetic composite. *Polym. Bull.* **2020**, *77*, 1049–1066. [[CrossRef](#)]
31. Sadeghi, M.; Irandoust, M.; Khorshidi, F.; Feyzi, M.; Jafari, F.; Shojaeimehr, T.; Shamsipur, M. Removal of arsenic (III) from natural contaminated water using magnetic nanocomposite: Kinetics and isotherm studies. *J. Iran Chem. Soc.* **2016**, *13*, 1175–1188. [[CrossRef](#)]
32. Weber, W.J.; Morris, J.C. Kinetics of adsorption on carbon from solutions. *J. Sanit. Eng. Div. Am. Soc. Civ. Eng.* **1963**, *89*, 31–60. [[CrossRef](#)]
33. Allen, S.; McKay, G.; Porter, J. Adsorption isotherm models for basic dye adsorption by peat in single and binary component systems. *J. Colloid Interface Sci.* **2004**, *280*, 322–333. [[CrossRef](#)] [[PubMed](#)]
34. Yimin, D.; Jiaqi, Z.; Danyang, L.; Lanli, N.; Liling, Z.; Yi, Z.; Xiaohong, Z. Preparation of Congo red functionalized Fe₃O₄@SiO₂ nanoparticle and its application for the removal of methylene blue. *Colloids Surf. A* **2018**, *550*, 90–98. [[CrossRef](#)]
35. Meng, C.; Zhikun, W.; Qiang, L.; Chunling, L.; Shuangqing, S.; Songqing, H. Preparation of ami-no-functionalized Fe₃O₄@mSiO₂ core-shell magnetic nanoparticles and their application for aqueous Fe³⁺ removal. *J. Hazard. Mater.* **2018**, *341*, 198–206. [[CrossRef](#)] [[PubMed](#)]